Optimization of displacement-measuring quadrature interferometers considering the real properties of optical components

Tomaž Požar,* Peter Gregorčič, and Janez Možina

Faculty of Mechanical Engineering, University of Ljubljana, Aškerčeva 6, 1000 Ljubljana, Slovenia

*Corresponding author: tomaz.pozar@fs.uni-lj.si

Received 5 November 2010; revised 19 January 2011; accepted 20 January 2011;
posted 24 January 2011 (Doc. ID 137749); published 10 March 2011

We present the influence of alignment and the real properties of optical components on the performance of a two-detector homodyne displacement-measuring quadrature laser interferometer. An experimental method, based on the optimization of visibility and sensitivity, was established and theoretically described to assess the performance and stability of the interferometer. We show that the optimal performance of such interferometers is achieved with the iterative alignment procedure described. © 2011 Optical Society of America

OCIS codes: 120.0120, 120.3180, 120.3930, 120.4570, 230.1360, 230.5440.

1. Introduction

Single-frequency, displacement-measuring laser interferometers based on quadrature detection are renowned for their accuracy, wide dynamic range, and constant sensitivity [1–5]. In order to maintain their long-term accuracy, these interferometers must be assembled in such a way that slight misalignments of the optical components do not significantly alter their performance [6,7]. The attainable accuracy of any homodyne quadrature laser interferometer (HQLI) is limited by three main sources of uncertainty: (i) the instability of the frequency and the amplitude of the laser source, including the uncertainty of the refractive index through which the laser beam propagates; (ii) real properties and imperfections of optical components and their performance under small mechanical displacements from their optimally aligned positions; and lastly (iii) the light-detection part of the interferometer with subsequent specific data processing to obtain the desired displacement from the raw photodiode signals.

The goal of this paper is to theoretically and experimentally investigate the influence of alignment and the real properties of optical components on the performance of a two-detector homodyne displacement-measuring quadrature interferometer built from commercially available optical components. For this purpose, we developed an experimental method to assess the performance and the stability of the interferometer against slight mechanical misalignments due to unwanted ambient vibrations or temperature shifts. It bases on measuring the values of the extremes of the interference curve for each photodiode output while rotating a wave plate through a full round trip. The phase shift between the two signals and their visibilities are also monitored.

The measured dependencies of the above-mentioned signal parameters on the angle of the wave-plate rotation indicate that if an additional phase shift originates from the polarization-sensitive light reflections, such as the reflection at the nonpolarizing beam splitter [6,8], the interferometer operates in a mechanically unstable regime even if it is aligned to minimize the nonlinearities that originate from an unequal AC amplitude, DC offsets, a lack of quadrature, and polarization cross talk.

0003-6935/11/091210-10$15.00/0

Furthermore, we show that it is not always possible to both attain the constant sensitivity (equal AC amplitudes and a 90° phase shift) and at the same time set the interferometer in the stable operating range.

2. Experimental Setup and Alignment of HQLI

Several errors in the detected displacement arise from misaligned or imperfect optical components [9,10]. With this in mind, we realized an experimental two-detector HQLI with a desire to simplify its alignment and to reduce the presence of nonlinearities for the aligned interferometer. A two-detector HQLI has the minimum number of optical components needed to obtain a pair of orthogonally polarized signals in phase quadrature: one beam splitter, one polarizing beam splitter, one octadic wave plate (OWP), and two reflective surfaces (e.g., reference and target mirrors).

The top view of our HQLI setup is schematically illustrated in Fig. 1. The cylindrical head of the linearly polarized and frequency-stabilized He–Ne laser (SIOS SL 02/1, $\lambda = 632.8\,\text{nm}$ in air, and the output power $P_0 \geq 1\,\text{mW}$) is rotated so that the linearly polarized beam exiting the laser lies in the plane of the optical table (x–z plane). After the optical

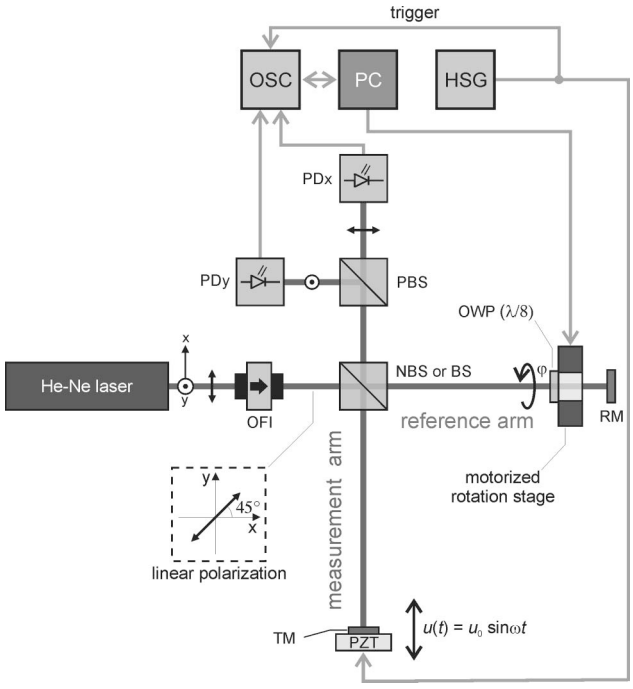

Fig. 1. Schematic top view of the ideal HQLI. The polarization states are designated as arrows on the beam. The optical components used are: an optical Faraday isolator (OFI), a nonpolarizing beam splitter (NBS) or beam splitter (BS), an octadic wave plate (OWP) mounted on the motorized rotation stage, a reference mirror (RM), a target mirror (TM) attached to the piezoelectric transducer (PZT), and a polarizing beam splitter (PBS). The two signals are detected with photodiodes (PDx and PDy) and acquired by the oscilloscope (OSC). The signal from the harmonic-signal generator (HSG) is current-amplified and used to drive the PZT. A personal computer (PC) runs the automated measurements and turns the motorized rotation stage.

Faraday isolator (OFI), the beam polarization forms a 45° angle with respect to the x axis. This polarization can be decomposed into two orthogonal polarizations with equal intensities, one in the plane of the paper (x axis) and the other perpendicular to it (y axis). The 50%–50% nonpolarizing cube beam splitter (NBS) or regular cube beam splitter (BS) evenly divide the beam into the reference and measurement arms. The reflection-to-transition ratio of the NBS is insensitive to the incoming polarization, while it is polarization-dependent for the BS. The first transition through the OWP, which is placed in the reference arm, gives rise to the 45° ($\lambda/8$) phase difference between the orthogonal polarizations. The beam is then reflected from the reference mirror (RM) and an additional 45° are added on to the returning passage through the OWP. The orthogonal polarizations in the measurement arm undergo an equal phase shift δ due to the movement of the target mirror (TM), which is driven by a piezoelectric transducer (PZT). The light in phase opposition is not detected, because it returns toward the laser and is blocked by the OFI to prevent any destabilization of the laser. The polarizing beam splitter (PBS) transmits the x-polarization and reflects the y-polarization.

Two beams with polarizations in the x–z plane, one from the reference arm and the other from the measurement arm, reach the Si photodiode PDx. The perpendicular polarizations coming from both arms are detected by the Si photodiode PDy. The two photodiodes are equal and have equal amplification gains. Furthermore, the arms are of equal length so that the interfering beams have the same wavefront curvature. Ideally, the interference signals on the photodiodes are shifted by 90°, which can be achieved with a properly rotated OWP. The measured displacement u is encoded in the phase $\delta(u) = 4\pi u/\lambda$, where λ is the wavelength of the interferometric laser in air.

A highly reflective TM is attached to the PZT (PI, PICMA PL055), which is driven by the current-amplified (PI, E-660 single-channel LVPZT amplifier) harmonic-signal generator (Tektronix, 100 MHz AFG 3102). The mirror vibrates with an amplitude of $u_0 = 200\,\text{nm}$ and a frequency of $f = 70\,\text{Hz}$. The displacement amplitude is high enough so that the whole fringe is detected on each photodiode. The OWP is carefully inserted into the motorized rotation stage (Eksma, 960-0140 with stepper motor FL42STH33-0404B, 0.4 A, 200 steps) so that the beam is perpendicular to the plate during its rotation. An automated software routine written in MATLAB rotates the stage in steps of 1°. For each position of the OWP, the raw photodiode signals are acquired from a digital oscilloscope (LeCroy, 500 MHz WaveRunner 6050A). The acquisition time is 20 ms, i.e., longer than the period of TM vibration. After the raw signals are obtained, the data are processed offline. The processing algorithm first determines and effectively corrects the common nonlinearities [11–13] and then unwraps the phase to obtain the displacement [14]. The extremes are

either read from the 2 kHz-low-pass filtered raw voltage signals as their maximum and minimum values or obtained from the retrieved free coefficients of the fit. These parameters are later used to determine the visibilities and the sensitivity of the interferometer.

A. Alignment of the HQLI

The main objective of mechanical alignment of components is to achieve conditions under which the interferometer will have the best performance. The alignment procedure consists of spatial guiding of beams, and altering polarization properties of the interfering beams. There are three measurable quantities that need to be optimized during the alignment procedure: the *visibilities* and *AC amplitudes* of both signals, which need to be maximized, and the *constant sensitivity*, which has to be approximated as closely as possible. A constant sensitivity requires the signals to have equal amplitudes and to be 90° phase-shifted. It is desirable to make use of as much light from the interferometric laser as possible, because the signal-to-noise ratio in the measured displacement is proportional to the square root of the laser power reaching the photodiodes. Signals with higher amplitudes also suffer less from the noise of the A/D converter when they are digitized. For this reason, the photodiode's output has to be amplified, since the responsivity of the Si photodiode at 633 nm is only 0.4 A/W. A 1 mW input power gives an amplified output of about 2 V if the transimpedance gain at a 50 Ω load is around 5 kV/A. The linear conversion gain of the input power to the output voltage of our photodiodes is $G = 2\,\mathrm{kV/W}$.

The choice of optical components influences the robustness/stability of the HQLI with respect to slight mechanical misalignments originating from shorter-term unwanted ambient vibrations or longer-term temperature shifts. For example, an additional phase shift originating from the polarization-sensitive light reflections, such as the reflection at the beam splitters, puts the interferometer into the unstable regime. The visibilities can also be significantly improved if the optical components used in the HQLI are optimized for the laser's wavelength [e.g., antireflection (AR)-coated optics].

We decided to analyze two distinct alignments of the interferometer. The first alignment procedure is called the *prealignment* because it is adjusted prior to inserting the OWP into the reference arm. This alignment is more intuitive because it is suggested by the basic scheme of the ideal HQLI that is illustrated in Fig. 1. In contrast, the second adjustment of the interferometer's components is dubbed the *postalignment*, because it is aligned after the OWP has been included. This alignment is iterative, and thus more time consuming, but yields a better-performing practical interferometer.

1. *Prealignment*

The main idea behind this alignment is to simulate the assembly of the HQLI as described by the basic scheme. A 45° angle between the polarization plane of the light and the plane of the optical table (x–z plane) can be adjusted by rotating the cylindrical laser head or by an additional half-wave plate. In fact, this angle must be measured according to the coordinate axes defined by the PBS.

When the path of the beam has been made parallel to the optical table and forms right angles on the (semi)reflective surfaces, the laser head has to be rotated to the position where the amplitudes of both signals on the photodiodes become equal. This is done by occluding the measurement arm. The photodiodes also have to be manually position-aligned so that their outputs are maximized. Then, the occlusion in the measurement arm is removed and the vibrating TM is angle-adjusted so that the interference signals have maximum (and equal) AC amplitudes and visibilities. Finally, the wave plate is inserted and rotated so that a quadrature is achieved between the signals. Ideally, this alignment should yield signals given by the Eqs. (2) in Section 3. In practice, this alignment does not lead to the optimum performance of the interferometer, as will be shown by the measurements.

2. *Postalignment*

The alignment of the HQLI after the wave plate has already been inserted into the beam path in the reference arm provides a better performance in the case of a practical interferometer with nonideal optical components. The main difference, compared to the prealignment, is that this adjustment method is iterative, i.e., the incoming polarization plane and the wave plate have to be iteratively rotated in order to converge to the desired optimization of the AC amplitudes, the visibilities, and the exact quadrature. In the case of a HQLI built from ideal components, both alignments are indiscernible and satisfy the requirements for optimal performance.

3. Theory

The operation of the two-detector HQLI (schematically illustrated in Fig. 1) with ideal optical components can be most conveniently described by the Jones matrix formalism on the propagation of plane light waves. The matrices describing the polarization properties of the used ideal optical components can be found in [4]. Employing this mathematical formalism, we here derive the dependence of the intensities I_x and I_y on the photodiodes PDx and PDy on the optical phase δ and on the angle of rotation φ of an arbitrary-retardation wave plate (WP) with a retardation difference n:

$$
\begin{aligned}
I_x(\delta, 2\varphi, n) &= \frac{I_0}{8}[(\cos\delta + \cos n)^2 + (\sin\delta \\
&\quad - \sin n(\cos 2\varphi + \sin 2\varphi))^2] \\
&= c_x + a_x \cos(\delta - \delta_{I_x}^{\max}), \\
I_y(\delta, 2\varphi, n) &= \frac{I_0}{8}[(\cos\delta + \cos n)^2 + (\sin\delta \\
&\quad + \sin n(\cos 2\varphi - \sin 2\varphi))^2] \\
&= c_y + a_y \cos(\delta - \delta_{I_y}^{\max}).
\end{aligned} \tag{1}
$$

Here, I_0 stands for the output intensity of the interferometric laser (the intensities in all of the equations may be replaced by powers). The angle φ is measured from the y axis to the WP's fast axis. Assuming a linear response of the photodiodes, the same dependence as in Eqs. (1) is expected in the measured amplified output voltages V_x and V_y from the photodiodes. It is also clear from Eqs. (1) that the intensities have a double period for a full revolution of the WP. We will show later in this article that the intensities I_x and I_y vary harmonically with respect to the optical phase δ, which can be formally written as a harmonic dependence on δ with the phase-independent DC offsets $c_{x,y}$, the AC amplitudes $a_{x,y}$, and the phase offsets $\delta_{I_x,I_y}^{\max}$.

To show the influence of alignment and the properties of optical components on the performance of HQLI, we will use Eqs. (1) to derive the following theoretical expressions: (i) formal equations showing that the intensities on the photodiodes are harmonically dependent on the optical phase δ; (ii) equations for the common nonlinearities $c_{x,y}$, $a_{x,y}$ and α as a function of φ and n; (iii) equations for the two figures of merit: the visibility of both signals (vis_x and vis_y) as a function of φ and n, and the sensitivity S for two-detector HQLI; and (iv) analytical expression for the sensitivity of the phase shift $d\alpha/d\varphi$ for an arbitrary-WP rotation and arbitrary retardation value.

Under ideal conditions, when the fast axis of the OWP ($n = \pi/4$) is perpendicular to the x–z plane ($\varphi = 0°$), the signals are in phase quadrature:

$$
\begin{aligned}
I_x(\delta - 45°, 0°, \pi/4) &= \frac{I_0}{4}(1 + \cos\delta), \\
I_y(\delta - 45°, 0°, \pi/4) &= \frac{I_0}{4}(1 + \sin\delta).
\end{aligned} \tag{2}
$$

A constant optical phase of 45° was subtracted from the varying optical phase δ in order to show that the signals on PDx and PDy vary as cosine and sine functions, respectively. Thus, the signals are in quadrature, i.e., are 90° out of phase.

The time-dependent displacement $u(t)$ of the TM along the line of the laser beam is encoded in the optical phase as $\delta(u(t)) = 4\pi u(t)/\lambda$ and is derived from the ideal quadrature signals $I_x(t)$ and $I_y(t)$ [Eqs. (2)] by subtracting the time-independent DC offsets $c_{x,y} = I_0/4$ as

$$
\begin{aligned}
u(t) &= \frac{\lambda}{4\pi}\left(\arctan\frac{I_y(t) - I_0/4}{I_x(t) - I_0/4} + m\pi\right), \\
m &= 0, \pm 1, \pm 2, \ldots .
\end{aligned} \tag{3}
$$

Here, λ stands for the laser wavelength in air. Note that the AC amplitudes $a_{x,y} = I_0/4$ divide out in the ideal case. The integer m must be chosen correctly, so that the function $u(t)$ satisfies the condition of being continuous.

The rotation of the WP has an influence on the phase shift between I_x and I_y, and their maximum and minimum values (or, equivalently, on their DC offsets and AC amplitudes). To calculate these values, we need to find the extremes of Eqs. (1) with respect to δ for an arbitrary angle φ and retardation difference n. The locations of the maxima are labeled $\delta_{I_x,I_y}^{\max}$, while the minima are labeled $\delta_{I_x,I_y}^{\min}$:

$$
\begin{aligned}
\delta_{I_x}^{\max}(2\varphi, n) &= -\arctan[\tan n(\sin 2\varphi + \cos 2\varphi)], \\
\delta_{I_x}^{\min}(2\varphi, n) &= \pi + \delta_{I_x}^{\max}, \\
\delta_{I_y}^{\max}(2\varphi, n) &= -\arctan[\tan n(\sin 2\varphi - \cos 2\varphi)], \\
\delta_{I_y}^{\min}(2\varphi, n) &= \pi + \delta_{I_y}^{\max}.
\end{aligned} \tag{4}
$$

Substituting the locations of the extremes [Eqs. (4)] back into Eqs. (1) gives the maximum and minimum values of the theoretically detectable intensities for arbitrary φ and n:

$$
\begin{aligned}
I_x^{\max}(4\varphi, n) &= I_x(\delta_{I_x}^{\max}, \varphi, n) = \frac{I_0}{8}\left(\sqrt{1 + k} + 1\right)^2, \\
I_x^{\min}(4\varphi, n) &= I_x(\delta_{I_x}^{\min}, \varphi, n) = \frac{I_0}{8}\left(\sqrt{1 + k} - 1\right)^2, \\
I_y^{\max}(4\varphi, n) &= I_y(\delta_{I_y}^{\max}, \varphi, n) = \frac{I_0}{8}\left(\sqrt{1 - k} + 1\right)^2, \\
I_y^{\min}(4\varphi, n) &= I_y(\delta_{I_y}^{\min}, \varphi, n) = \frac{I_0}{8}\left(\sqrt{1 - k} - 1\right)^2,
\end{aligned} \tag{5}
$$

introducing $k(4\varphi, n) = \sin^2 n \sin 4\varphi$, having a fourfold period per full revolution of the WP.

The relation between the phase shift α and the angle of an arbitrary-WP rotation is defined as the difference between $\delta_{I_y}^{\max,\min}$ and $\delta_{I_x}^{\max,\min}$:

$$
\begin{aligned}
\alpha(2\varphi, n) &= \arctan[\tan n(\cos 2\varphi - \sin 2\varphi)] \\
&\quad + \arctan[\tan n(\cos 2\varphi + \sin 2\varphi)],
\end{aligned} \tag{6}
$$

while the sensitivity of the phase shift on the arbitrary-WP rotation corresponds to the slope $d\alpha/d\varphi$, which can be extracted from Eq. (6) as

$$
\frac{d\alpha}{d\varphi} = \frac{4\tan n \sin 2\varphi[1 + \cos 4\varphi - \cos^{-2} n(2 + \cos 4\varphi)]}{1 + 2\tan^2 n + \tan^4 n \cos^2 4\varphi}. \tag{7}
$$

From Eqs. (5) we obtain the DC offsets

$$c_x(4\varphi,n)=\frac{I_x^{\max}+I_x^{\min}}{2}=I_0\frac{2+k}{8},$$
$$c_y(4\varphi,n)=\frac{I_y^{\max}+I_y^{\min}}{2}=I_0\frac{2-k}{8}, \tag{8}$$

and AC amplitudes

$$a_x(4\varphi,n)=\frac{I_x^{\max}-I_x^{\min}}{2}=I_0\frac{\sqrt{1+k}}{4},$$
$$a_y(4\varphi,n)=\frac{I_y^{\max}-I_y^{\min}}{2}=I_0\frac{\sqrt{1-k}}{4}. \tag{9}$$

The visibility is a standard figure of merit for an interferometer and is defined as

$$\mathrm{vis}_x(4\varphi,n)=\frac{a_x}{c_x}=\frac{I_x^{\max}-I_x^{\min}}{I_x^{\max}+I_x^{\min}}=\frac{2\sqrt{1+k}}{2+k},$$
$$\mathrm{vis}_y(4\varphi,n)=\frac{a_y}{c_y}=\frac{I_y^{\max}-I_y^{\min}}{I_y^{\max}+I_y^{\min}}=\frac{2\sqrt{1-k}}{2-k}. \tag{10}$$

Here, $\mathrm{vis}_{x,y}$ stand for the visibility of both signals. The values $I_{x,y}^{\min}$ [Eqs. (5)] are in general not zero, because the destructive interference of the beams coming from both interferometric arms is not perfect even from the theoretical point of view.

We expect that in the case of an ideal HQLI, the signal parameters $c_{x,y}$, $a_{x,y}$, and $\mathrm{vis}_{x,y}$ contain a fourfold period in a full revolution of the WP, while the phase difference between the signals α has a double period.

The sensitivity S is defined as the derivative of the signal with respect to the displacement. For a two-detector interferometer, it is equal to the square root of the sum of the squared sensitivities of both channels:

$$S=\sqrt{S_x^2+S_y^2}=\left[\left(\frac{dV_x}{du}\right)^2+\left(\frac{dV_y}{du}\right)^2\right]^{1/2}. \tag{11}$$

Inserting Eqs. (1) into Eq. (11) gives

$$\begin{aligned}S&=\frac{4\pi G}{\lambda}\left[\left(\frac{d}{d\delta}(c_x+a_x\cos(\delta-\delta_{I_x}^{\max}))\right)^2\right.\\&\quad\left.+\left(\frac{d}{d\delta}(c_y+a_y\cos(\delta-\delta_{I_y}^{\max}))\right)^2\right]^{1/2}\\&=\frac{4\pi G}{\lambda}[a_x^2\sin^2(\delta-\delta_{I_x}^{\max})+a_y^2\sin^2(\delta-\delta_{I_y}^{\max})]^{1/2}.\end{aligned} \tag{12}$$

If the AC amplitudes are equal ($a_{x,y}=a$) and the phases are in quadrature ($\delta_{I_y}^{\max}=\delta_{I_x}^{\max}+90°$), then the sensitivity is constant, i.e., independent of the optical phase δ, and equal to the one-half of the highest attainable sensitivity of a Michelson interferometer operating at the midpoint between the signal's maximum and minimum:

$$\begin{aligned}S&=\frac{4\pi G}{\lambda}[a^2\sin^2(\delta-\delta_{I_x}^{\max})\\&\quad+a^2\sin^2(\delta-(\delta_{I_x}^{\max}+90°))]^{1/2}\\&=\frac{4\pi Ga}{\lambda}[\sin^2(\delta-\delta_{I_x}^{\max})+\cos^2(\delta-\delta_{I_x}^{\max})]^{1/2}\\&=\frac{4\pi Ga}{\lambda}.\end{aligned} \tag{13}$$

Thus, a constant sensitivity corresponds to the Lissajous figure of the raw signals when they form a circle. On the other hand, a lack of quadrature and/or unequal AC amplitudes distort this circle into an ellipse centered at (c_x,c_y) [15].

4. Results and Discussion

A. Pre- and Postaligned Signals

The distance measured with the HQLI is obtained from two signals that have a phase shift α. This phase shift depends on the angle of the OWP rotation φ and, in practice, on the additional phase shift α_0 that originates from polarization-sensitive light reflections on optical components. Equations (8) and (9) imply that the rotation of the OWP not only changes the phase shift between the signals, but it also influences the AC amplitudes and DC offsets. Therefore, the performance of the interferometer depends on the alignment procedure if the additional phase shift is present.

Figure 2(a) shows both signals obtained at the stage before the OWP is placed into the HQLI during the prealignment procedure. In this case we used a NBS, which adds an additional phase shift for the normal beam incidence $\alpha_{0\perp}=57.5°$ into the system. Because of the lack of quadrature between the signals [Fig. 2(a)], the Lissajous curve, shown in Fig. 2(c), forms an ellipse. This extra phase shift, originating from the beam splitter, is obtained by fitting the ellipse. Figure 2(a) also shows that both signals have equal amplitudes at this stage of the prealignment procedure. The quadrature of these signals ($\alpha=90°$) is achieved when the OWP is placed into the reference arm of the HQLI and rotated by $\varphi=27°$, as can be seen in Fig. 3(a) [the vertical dotted line (1) intersecting the full circles]. In this case, the accomplished prealignment gives phase quadrature, but the signals no longer have equal AC amplitudes and DC offsets. Therefore, the visibility is reduced and the sensitivity is no longer constant.

On the other hand, constant sensitivity and maximum visibilities can be achieved at the same time by using the postalignment procedure. Figure 2(b) shows both signals obtained after the HQLI has been postaligned. In this case, the signals with equal amplitudes are in quadrature and their parametric representation in Fig. 2(c) forms a circle, i.e., the HQLI operates at constant sensitivity. Although the sensitivity and visibility can be optimized with the postalignment technique, the interferometer is sensitive

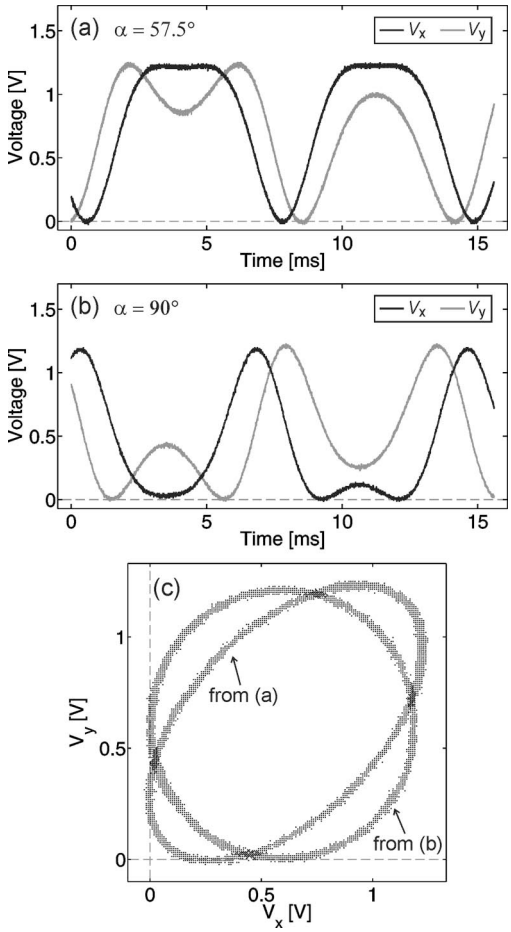

Fig. 2. Comparison between the measured photodiode signals obtained with (a) a prealigned interferometer without OWP and (b) a postaligned interferometer in quadrature. (c) The parametric Lissajous representation of the measured signals. The ellipse is obtained from (a) and the circle from (b).

to mechanical disturbances, as will be discussed in the next subsection.

B. Robust Realization of HQLI

The solid curve in Fig. 3(a) shows the theoretical dependence $\alpha(\varphi)$ for the HQLI with ideal components [Eq. (6) for $n = \pi/4$]. As the polarization-sensitive light reflections at certain optical elements provide an additional and constant phase shift, such as the reflection at a beam splitter, an extra constant term α_0 has to be added to the right-hand side of Eq. (6). To show and explain the origin of this extra phase shift, the measurements were carried out with two different beam splitters.

A NBS that adds an extra phase shift of 57.5° for the normal beam-incidence was used in the first three series of measurements. The first series [cross symbols in Fig. 3(a)] was performed with the *postaligned* interferometer, while the other series were made with the *prealigned* interferometer. In contrast to the second series [filled circles in Fig. 3(a)], the NBS was rotated by 180° around the y axis in the measurements of the third series [open circles in Fig. 3(a)]. In this case, $\alpha_{0\perp}$ changes sign. This proves that the NBS is asymmetric on the rotation by 180° around the y axis. If the quadrature has a negative sign [e.g., vertical dotted line (5) in Fig. 3], the signals V_x and V_y must be interchanged so that the direction of the measured displacement has the right sign. The fourth series [filled squares in Fig. 3(a)] was performed with a BS adding $\alpha_{0\perp} = 15°$.

We measured the dependence of α_0 on the incident angle ϑ_{NBS}. This small angle is defined with respect to the normal to the beam splitter's face and is positive when the beam reflects from the internal partially reflecting surface by an angle greater than the right angle. During the measurements of α_0, the OWP was removed from the interferometer. Figure 4 shows the $\alpha_0(\vartheta_{\mathrm{NBS}})$ dependence. This measurement implies that the rotation misalignment around the y axis of the NBS by only 1° gives rise to a 10° change in the inherent NBS phase difference α_0. As the NBS cube is made from nonbirefringent BK7 glass, the phase difference arises entirely from the asymmetric dielectric coatings on the protected internal surface. It would be useful to design commercial specialized nonpolarizing beam splitters for polarization-based interferometry with either $\alpha_{0\perp} = 0°$ or $\alpha_{0\perp} = 90°$. In the latter case, a suitable wave retarder is redundant, thus the number of optical components can be further reduced.

The theoretical sensitivity of the phase shift on the OWP rotation, which corresponds to the slope $d\alpha/d\varphi$ [Eq. (7)], is shown in Fig. 3(b). A robust realization of an interferometer should minimize the influence of slight mechanical displacements/rotations of the optical components from their aligned positions on the nonlinearities. In the HQLI, the robustness can be achieved by using an ideal OWP with the nominal retardation value of $\lambda/8$, while the other optical components must not contribute any extra phase shift between the polarizations. If this is achieved, the value $d\alpha/d\varphi = 0$ for an ideal 90° phase shift, as is shown by the vertical dotted line (4) in Fig. 3. Therefore, the phase shift in such an interferometer is insensitive to slight OWP rotations.

On the other hand, when the constant value of the phase shift α_0 originates from the beam splitter, the OWP is used to add only the remaining phase shift, which is needed to attain the quadrature. As a consequence, such an interferometer is more sensitive to OWP rotation. This is shown by the vertical dotted lines (1), (2), (3), and (5) in Fig. 3. Although the value of $\alpha_{0\perp}$ is crucial for the robust realization of homodyne quadrature interferometers, it is not available in commercial catalogs [16,17]. In the worst-case scenario, a rotation of 1° of the angle φ changes the phase shift by about 3°, which results in an error for the measured distance. This gives the displacement-error amplitude of about 3 nm [4] in the described single-pass, two-detector HQLI.

It can be concluded from the results in Fig. 3 that the robust realization of a HQLI requires optical components that do not provide any additional

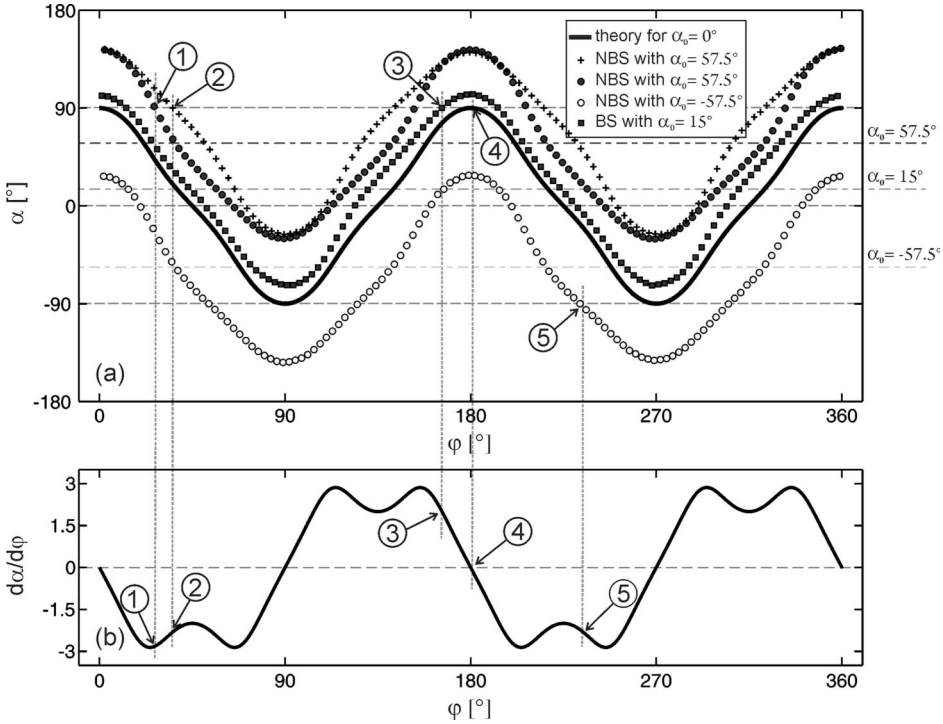

Fig. 3. Dependence of the phase shift α on the OWP angle φ. (a) The solid curve shows the theoretical curve [Eq. (6)] for the HQLI with ideal components. The crosses and filled circles show the measurements of $\alpha(\varphi)$ for the NBS with an additional phase shift $\alpha_0 = 57.5°$ in the case of a post- and prealigned HQLI, respectively. The open circles show the same dependence, when the same NBS was rotated by 180° around the y axis in the prealigned HQLI. Filled squares show the measurement of $\alpha(\varphi)$ for the BS with $\alpha_0 = 15°$ placed in the prealigned interferometer. (b) The theoretical sensitivity of the phase shift on the OWP rotation [Eq. (7)].

constant phase shifts due to the polarization-sensitive light reflections. In this case, the theory for an arbitrary-WP [Eq. (7)] implies that the OWP ($n = \pi/4$) is the best choice for the ideal HQLI presented in Fig. 1. On the other hand, when the additional constant phase shift is present, the robust realization of a HQLI requires a custom-made WP with an appropriate retardation.

Special care is needed to ensure that the manufactured retardation value is equal to or (slightly) greater than the optimal one. Otherwise, the quadrature cannot be achieved [15]. Although the lack of quadrature can be determined and corrected with appropriate signal processing, it always ruins the constant sensitivity, as a result of which the resolution of the interferometer varies with the measured distance. Moreover, an inappropriate phase shift also results in an unwanted reduction of visibility in both signals. Therefore, the reduction of the phase-shift nonlinearity in quadrature-detection-based interferometers has priority over the sensitivity of crucial optical components on their mechanical changes, such as the rotation of the OWP.

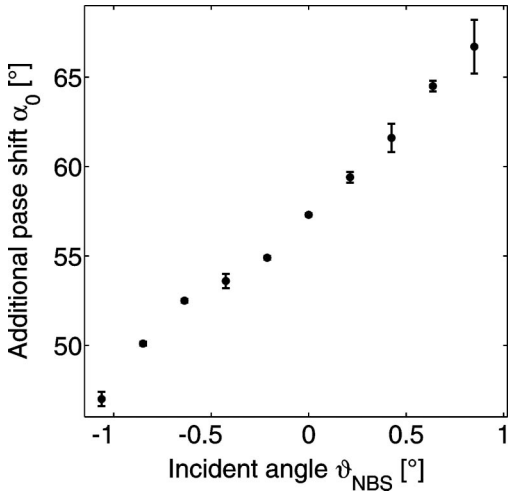

Fig. 4. Dependence of the inherent phase shift α_0 originating from the NBS as a function of the incidence angle ϑ_{NBS}. Each point is an average of 10 measurements.

C. Visibility

We first consider the general behavior of an ideal HQLI in order to analyze the parameters of the interference signals when an OWP is rotated around its axis. Figure 5 shows how the theoretical maximum and minimum [Eqs. (5)] of both signals, and consequently their visibilities [Eqs. (10)], vary as a function of the OWP rotation angle. The results in Fig. 5(a) are scaled so that they can be compared to the measurements obtained with our HQLI. The OWP gives a proper absolute value of the phase shift of 90° at $\varphi = 0°$, 90°, 180°, and 270° (shown with the vertical dotted lines in Fig. 5). Whenever the quadrature is achieved, the minimum of both signals drops to 0 V and, consequently, the visibilities are maximized to 1.

Note that for every φ where the OWP gives no retardance between the signals, the visibilities are also maximized and both signals have equal AC amplitudes. For all other positions of the OWP, the visibilities are smaller than 1, and the AC amplitudes become unequal. The quantities presented in Fig. 5 have a fourfold period for a full revolution of the OWP.

The dependences of the maximum, the minimum, and the visibility of both signals on the OWP rotation angle φ were measured with our HQLI using two alignment techniques and two different beam splitters: the BS and the NBS. The results are shown in Figs. 6–8 for the prealigned HQLI with the NBS (Fig. 6), the prealigned HQLI with the BS (Fig. 7), and the postaligned with NBS (Fig. 8).

The results in Figs. 6 and 7 show that a prealigned HQLI (with either the NBS or BS) has reduced visibilities and unequal AC amplitudes when the signals are in phase-quadrature. It has to be additionally emphasized that high visibilities can only be obtained if special attention is given to aligning the interfering beams so that there is no parallel or angular shift between them. Moreover, the visibilities also depend on the unequal reflectivity of the mirrors, the different wave-front curvatures between the interfering beams (unequal arm lengths), the temporal coherence, ghost images, AR coatings, the flatness of optical components, etc. Our NBS is AR coated for 633 nm [17], while the BS has no coatings

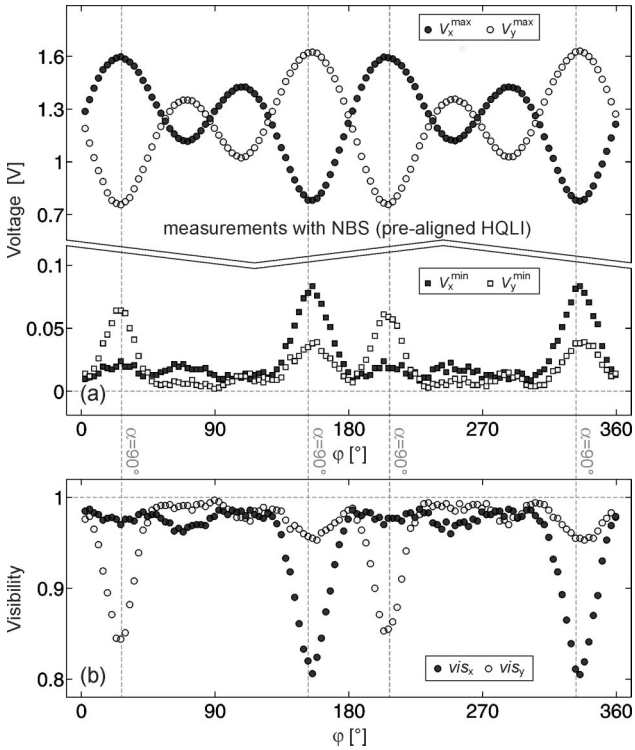

Fig. 6. Measured results for the prealigned HQLI with the NBS. (a) The maximum and minimum, and (b) the visibility of both signals as a function of the OWP rotation angle. The vertical dotted lines indicate the values of φ where the quadrature is achieved.

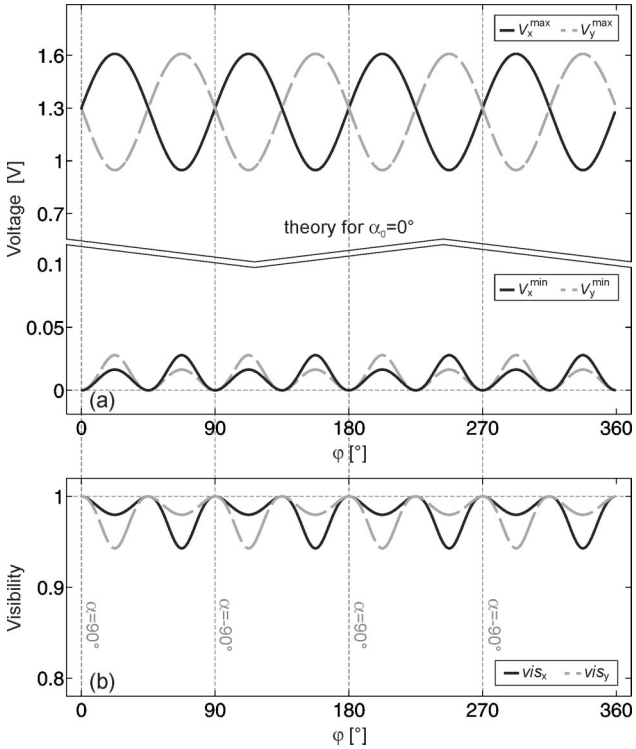

Fig. 5. Theoretical results for the ideal HQLI. (a) The maximum and minimum, and (b) visibility of both signals as a function of the OWP rotation angle. The curves are obtained from Eqs. (5) and (10) for OWP ($n = \pi/4$). The value of I_0 is replaced with 2.6 V.

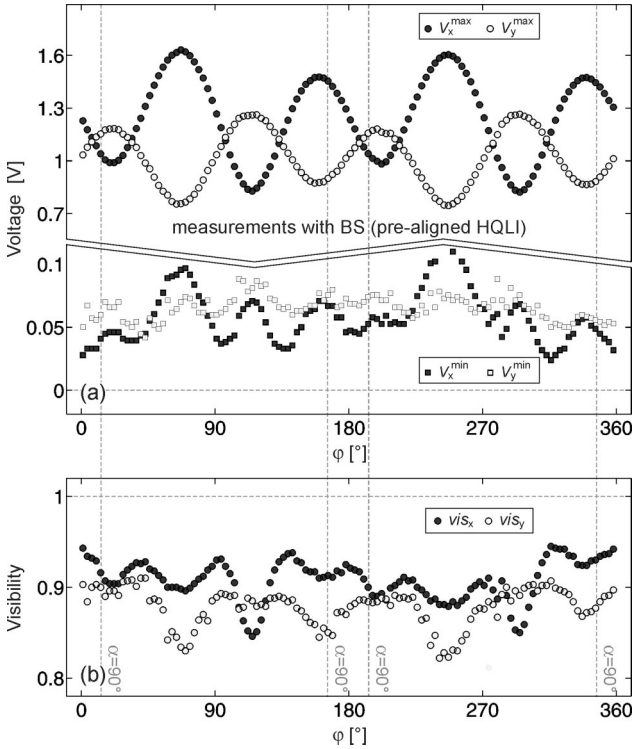

Fig. 7. Measured results for the prealigned HQLI with the BS. (a) The maximum and minimum, and (b) the visibility of both signals as a function of the OWP rotation angle. The vertical dotted lines indicate the values of φ where the quadrature is achieved.

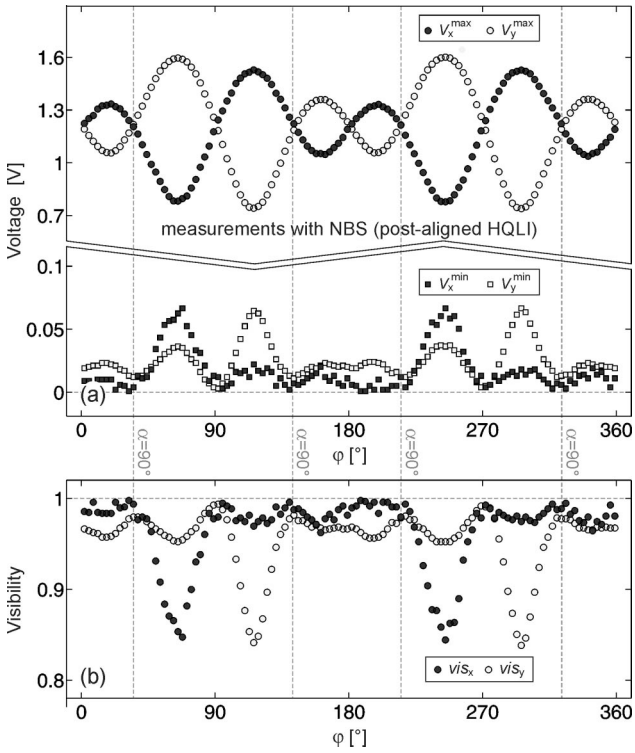

Fig. 8. Measured results for the postaligned HQLI with the NBS. (a) The maximum and minimum, and (b) the visibility of both signals as a function of the OWP rotation angle. The vertical dotted lines indicate the values of φ where the quadrature is achieved.

and, for this reason, the visibilities obtained with the BS are in general lower than with the NBS (compare Figs. 6 and 7).

The measured results differ slightly from the theory of the HQLI with ideal optical components. Because of the additional phase shift of the beam splitters, the quadrature is achieved at different angles φ in comparison with the ideal case (see the vertical dotted lines in Fig. 3); therefore, the vertical dotted lines in Figs. 6–8 are no longer separated by 90°. The fourfold symmetry is changed to a double period per full rotation of the OWP. This happens when the additional phase shift is present in combination with the polarization cross talk. This effect is more pronounced for the NBS ($\alpha_{0\perp} = 57.5°$), which gives a larger additional phase shift compared to the BS ($\alpha_{0\perp} = 15°$).

As is clear from Fig. 8, the postalignment technique has to be used in order to obtain optimal visibilities when phase-quadrature is achieved in a practical HQLI. Postalignment implies that the entering polarization is no longer 45° with respect to the x–z plane. Similarly, the tendency with postalignment is to equalize the AC amplitudes of both signals, which also yields better visibilities. Consequently, the fourfold symmetry is distorted so that the visibility is the highest when the signals are in phase-quadrature. Note that there is a slight shift between the vertical dotted lines (1) and (2) in Fig. 3. This happens because the measured $\alpha(\varphi)$ curves that were obtained using the NBS with two distinct alignment techniques [crosses and filled circles in Fig. 3(a)] differ. The reason for this is attributed to the unequal angles of the incoming linear polarizations required by the alignment instructions. The lines that correspond to the vertical dotted lines (1) and (2), although drawn four times, are seen in Figs. 6 and 8, where two different alignments are presented for the same NBS.

The experimental results obtained with the presented measuring method imply that a practical interferometer must be aligned with the described postalignment procedure to obtain high visibility in both signals and a constant sensitivity.

D. Sensitivity

The sensitivity is defined by Eq. (11) and can be measured from the output signals if the displacement of the TM is known. In our case, the TM was vibrating harmonically, as is shown in Fig. 9(a). The theoretical sensitivity of the HQLI is described by Eq. (12) and implies that the sensitivity depends only on the phase shift and the AC amplitudes of the acquired signals. We experimentally confirmed this by measuring the sensitivity for the three special cases: for the prealigned interferometer without OWP, where the signals with equal AC amplitudes are out of quadrature, i.e., $\alpha_{0\perp} = 57.5°$ [triangles in Fig. 9(b)]; the prealigned HQLI, i.e., the signals in quadrature have different AC amplitudes [circles in Fig. 9(b)]; and for the postaligned interferometer [crosses in Fig. 9(b)]. In the last case, the signals are in quadrature and have equal AC amplitudes. Thus, the sensitivity is constant and—in our HQLI—equals 12 mV/nm.

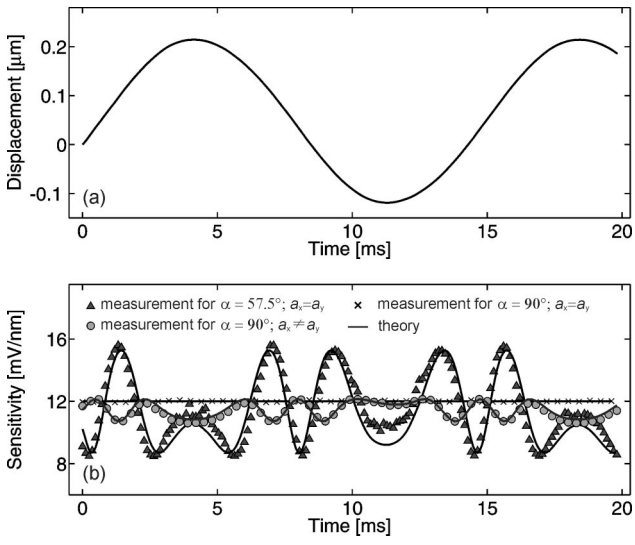

Fig. 9. (a) Displacement of the target mirror. (b) The measured sensitivities, corresponding to the given displacement, for: the prealigned HQLI without OWP, i.e., the signals have equal amplitudes, but are lacking the quadrature (triangles); the prealigned HQLI, i.e., the signals are in quadrature, but have different amplitudes (circles); and the postaligned HQLI, i.e., the signals in quadrature have equal amplitudes (crosses). The corresponding theoretical sensitivities are shown with the solid curves.

The theoretical sensitivities for all cases are shown in Fig. 9(b) with the solid black curves. Here, the theoretical curve is scaled to the experimental data. The scaling of Eq. (12) requires the extraction of parameters $a_{x,y}$ and δ_{I_x,I_y}. The values of $a_{x,y}$ were obtained from the maximum and minimum values of the acquired and low-pass filtered signals, while the coefficients δ_{I_x,I_y} were derived from the phase shift obtained using the data-processing algorithm. The optical phase $\delta(t)$ was derived from the measured displacement.

From the results presented in Fig. 9, it follows that: (i) There is a good agreement between the measured and the theoretical sensitivities. (ii) The constant sensitivity is achieved only when the following conditions: the quadrature and equal AC amplitudes of both signals are simultaneously fulfilled, (iii) otherwise it varies periodically with the optical phase. Consequently, (iv) the constant sensitivity (in the real HQLI) is only achieved in the postaligned interferometer.

5. Conclusion

We have presented theoretical and experimental results describing the influence of alignment and the properties of real optical components on the visibility, sensitivity and robustness of displacement-measuring quadrature interferometers. The performance of these interferometers was experimentally investigated using a single-pass, two-detector homodyne quadrature laser interferometer. The developed measuring technique employs a motorized rotation of the wave plate to achieve continuously varying phase shift. We have shown that the rotation of the wave plate produces unequal signal amplitudes, different zero offsets, and an unwanted visibility reduction in both signals.

Two basic alignment procedures (pre- and postalignment) were presented and analyzed. In the case of ideal optical components, there is no difference between these two alignments. But in a real case, when real optical components (e.g., with cross talk and an additional constant phase shift) are used, the choice of alignment procedure is important. In this case, the prealigned procedure leads to the reduction of visibilities and ruins the constant sensitivity. We have shown that the optimal performance of the interferometer (constant sensitivity and the maximization of the visibility in both channels) is assured by the postalignment procedure.

For the robust realization of the interferometer based on quadrature detection, any slight deviations of the optical components from their aligned positions should not significantly increase the nonlinearities. As an example, we have shown that an additional phase shift originating from the beam splitter leads in the worst-case scenario to a 3 nm displacement-error amplitude if the OWP in the HQLI is misaligned by 1°.

References

1. D. Y. Lee, D. M. Kim, D. G. Gweon, and J. Park, "A calibrated atomic force microscope using an orthogonal scanner and a calibrated laser interferometer," Appl. Surf. Sci. **253**, 3945–3951 (2007).
2. I. Misumi, S. Gonda, O. Sato, K. Sugawara, K. Yoshizaki, T. Kurosawa, and T. Takatsuji, "Nanometric lateral scale development using an atomic force microscope with directly traceable laser interferometers," Meas. Sci. Technol. **17**, 2041–2047 (2006).
3. T. Hausotte, B. Percle, and G. Jäger, "Advanced three-dimensional scan methods in the nanopositioning and nanomeasuring machine," Meas. Sci. Technol. **20**, 084004 (2009).
4. P. Gregorčič, T. Požar, and J. Možina, "Quadrature phase-shift error analysis using a homodyne laser interferometer," Opt. Express **17**, 16322–16331 (2009).
5. T. Požar and J. Možina, "Homodyne quadrature laser interferometer applied for the studies of optodynamic wave propagation in a rod," Strojniški Vestnik—J. Mech. Eng. **55**, 575–580 (2009).
6. F. Petrů and O. Číp, "Problems regarding linearity of data of a laser interferometer with a single-frequency laser," Precis. Eng. **23**, 39–50 (1999).
7. T. Keem, S. Gonda, I. Misumi, Q. X. Huang, and T. Kurosawa, "Simple, real-time method for removing the cyclic error of a homodyne interferometer with a quadrature detector system," Appl. Opt. **44**, 3492–3498 (2005).
8. J. J. Monzon and L. L. Sanchezsoto, "Absorbing beam splitter in a Michelson Interferometer," Appl. Opt. **34**, 7834–7839 (1995).
9. C. M. Wu and C. S. Su, "Nonlinearity in measurements of length by optical interferometry," Meas. Sci. Technol. **7**, 62–68 (1996).
10. J. Ahn, J. A. Kim, C. S. Kang, J. W. Kim, and S. Kim, "A passive method to compensate nonlinearity in a homodyne interferometer," Opt. Express **17**, 23299–23308 (2009).
11. P. Křen, "Linearisation of counting interferometers with 0.1 nm precision," Int. J. Nanotechnology **4**, 702–711 (2007).
12. P. L. M. Heydemann, "Determination and correction of quadrature fringe measurement errors in interferometers," Appl. Opt. **20**, 3382–3384 (1981).
13. M. A. Zumberge, J. Berger, M. A. Dzieciuch, and R. L. Parker, "Resolving quadrature fringes in real time," Appl. Opt. **43**, 771–775 (2004).
14. M. Dobosz, T. Usuda, and T. Kurosawa, "The methods for the calibration of vibration pick-ups by laser interferometry: part I. Theoretical analysis," Meas. Sci. Technol. **9**, 232–239 (1998).
15. P. Gregorčič, T. Požar, and J. Možina, "Phase-shift error in quadrature-detection-based interferometers," Proc. SPIE **7726**, 77260X (2010).
16. Edmund Optics, *Optics and Optical Instruments Catalog* (2010), p. 141.
17. Eksma Optics, *Laser Components 2009/2010* (2009), vol. 18, p. 1.39.